Proceedings of the 7th International Symposium on Fluid-Structure Interaction,
Flow-Sound Interaction, Flow-Induced Vibration and Noise

August 1-4th, 2010, Montreal, Canada

FEDSM-ICNMM2010-30075

FLOW CONDITIONS AT THE INLET OF ASPIRATING PIPES: PART 2 - EXPERIMENTS

Vincent Debut
Instituto Tecnologico e Nuclear (ITN/ADL)
Sacavem, Portugal

Jose Antunes
Instituto Tecnologico e Nuclear (ITN/ADL)
Sacavem, Portugal

François Axisa
Visiting researcher at ITN/ADL
Paris, France

ABSTRACT

Following the theoretical work and experimental strategy devised by Axisa (2010) in the companion paper, a test rig was designed and built in order to validate the analytical analysis of Part 1. Two configurations of partly immersed articulated pipes were tested, both for normal (expelling) and for reversed (aspirating) flows. The low-pressure water-loop enabled velocities up to 3 m/s in both normal and reversed flows, with no cavitation arising in the test section. The experimental results presented pertain to the following pipe configurations: (a) One articulated pipe, with either a common protruding or a rounded baffled free end; and (b) Two articulated pipes with equal lengths. For all flow velocities modal identifications were performed from the measured system responses.

The results obtained under normal expelling flow are in good agreement with the theoretical model originally developed by Benjamin (1961), which is also reviewed in Part 1. For the single articulated pipe, the Coriolis force term leads to a steady increase of damping with the flow velocity, modal frequency being significantly affected only near critical damping, as expected. For the two articulated pipes configuration, both the Coriolis and centrifugal flow terms are significant, leading to large changes in both modal frequencies and damping, which follow the predictions from the classical model.

The most interesting results from our experiments obviously concern the reversed aspirating flows. Following the discussion of Part 1, it was found that the one-pipe configuration is nearly insensitive to aspirating flows, irrespectively of the pipe termination geometry, showing that the Coriolis force term is canceled exactly by the term arising from the change in momentum of the flow entering the pipe at the free end. The experimental results from the two-pipes configuration are sensitive to the aspirating flow velocity. Among the various inflow models explored in Part 1, the one which assumes an inflow velocity directed along the tube axis, but without the tangential component of the pipe motion, proved to capture many of the features displayed by the experimental results. Actually, as the aspirating velocity increases, both identified modal frequencies of the two-pipes system, as well as the modal damping of the first mode, closely follow the theoretical predictions from such basic inflow model. However, a discrepancy was observed, concerning the modal damping trend of the second mode, which decreases slowly but steadily in our tests as the velocity increases, while the basic inlet flow model predicts a nearly constant damping value. Nevertheless, such subtle but significant behavior of the system damping can be related to small variations of the basic parameters which describe the inlet flow field.

1 INTRODUCTION

Most of the available experimental work on the dynamics of structures subjected to reverse flows addresses the reverse sprinkler problem, popularized by Feynman (1985), which triggered a significant number of publications – see Hsu (1988), Berg & Collier (1989), Lindgren (1990), Collier et al. (1991) , as well as the recent experiments by Païdoussis & Tétreault-Friend (2009). The reverse sprinkler problem is discussed in detail by Axisa (2010) in the companion paper, who also reports our own experimental efforts related with this topic, therefore the above-mentioned papers are barely recalled here.

Concerning pipes subjected to reverse internal flows, the currently available experimental work amounts to a limited number of publications, namely the work by Hongwu & Junji (1996), the early experiments referred by Païdoussis (1998) and the recent work by Kuiper & Metrikine (2008), as well as the experiments performed at McGill by Giacobbi (2007) and Rinaldi (2009), which are mentioned in the paper by Païdoussis & Tétreault-Friend (2009). Most of these work, which shows that the interest of the scientific community in this problem is very much alive, is also discussed in the companion paper.

Here, following the theoretical work and experimental strategy devised in Part 1, a test rig was designed and built in order to validate the analytical predictions. We briefly recall that, because the flow inlet conditions are at the heart of the difficulties in understanding the dynamics of aspirating pipes, the tested structures have been simplified as much as possible. Experiments using simple articulated systems of rigid pipes, with only one or two degrees of freedom, subjected to planar motions, can then be formulated in a straightforward manner, to highlight the relevant fluid dynamic effects of interest. This should enable us to supply first estimates of the crucial inflow parameters α, β, γ and π_p, which were defined and discussed in Part 1. The first three free parameters refer to the hypothesized unknown velocity of the flow entering the pipe:

$$\vec{V}_{out} = V_f\left(\alpha\vec{i} + \beta\frac{\partial Z}{\partial x}\vec{k}\right) + \gamma\frac{\partial Z}{\partial t}\vec{k} \qquad (1)$$

while π_p is a dimensionless pressurization coefficient.

The articulated pipes used in our experiments are, basically, systems analogue to those addressed by Benjamin (1961a,1961b). However, he did not perform any experiments under aspirating flow and, to our best knowledge, no one ever addressed the reversed flow problem by looking at the dynamics of articulated pipes. Furthermore, as far as we know, no quantitative data exists on the changes of the modal properties, as a function of the flow velocity, in pipe systems subjected to reverse flows. Neither any such quantitative experimental data has been produced, we believe, when the tube inlet geometry is changed in order to accommodate different singular head-losses, as discussed y Axisa (2010).

For the present work, two configurations of partly immersed articulated pipes were tested, both for normal (expelling) and for reversed (aspirating) flows. The low-pressure water-loop enabled velocities up to 3 m/s in both normal and reversed flows, with no cavitation arising in the test section. For all flow velocities modal identifications were performed from the measured system responses. The experimental results presented pertain to the following pipe configurations: (a) One articulated pipe, with either a common protruding or a rounded baffled free end; and (b) Two articulated pipes with equal lengths. For all flow velocities modal identifications were performed from the system responses measured using a displacement transducer and a laser vibrometer. These experimental results are then compared with the theoretical models discussed in Part 1, with an overall satisfactory agreement.

2 EXPERIMENTAL RIG AND TEST PROCEDURES

A general view of the experimental rig is shown in Figure 1 (a). The tested pipes are partially immersed in a water reservoir with dimensions $40 \times 40 \times 120$ cm. Water flow in the test loop is generated by three 1 kW electrical pumps, with a precise velocity controller. Most of the water loop consists on $1''$ plastic pipes, built with stiff spiral reinforcement, in order to avoid collapsing of the pipes subjected to suction. The flow rate is measured using an electronic flow meter and, overall, the axial flow velocity in the pipes – in the range $-3 \le V_f \le 3$ m/s – is estimated within ±5 % accuracy.

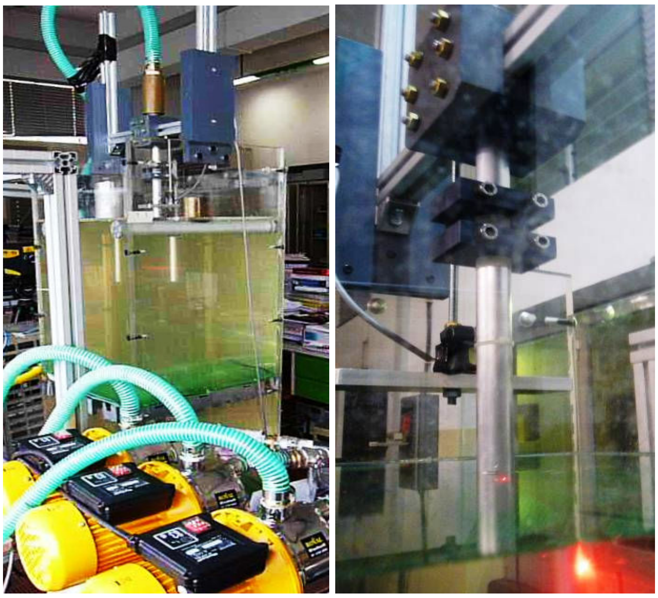

Figure 1. *(a) General view of the test rig; (b) Experimental configuration with one articulated pipe*

Figure 1 (b) shows the one-pipe tested configuration, consisting in a single aluminum pipe with structural mass $M_1 = 57.7$ g and length $L_1 = 300$ mm, internal diameter $D_{\text{int}} = 17.3$ mm and external diameter $D_{\text{ext}} = 19.9$ mm, which is suspended from a flexible "knee" allowing only planar motions. The lower part of the tube is immersed in the water tank, with an immersed height of $H_1 = 170$ mm. Figure

2 displays the two-pipe configuration tested, which consists in two articulated pipes with equal masses $M_1 = M_2 = 51.9\ \text{g}$ and lengths $L_1 = L_2 = 300\ \text{mm}$, diameters $D_{\text{int}} = 17.5\ \text{mm}$ and $D_{\text{ext}} = 19.9\ \text{mm}$, the lower pipe height $H_2 = 100\ \text{mm}$ being immersed in the water tank.

At the bottom of the water reservoir, a settling chamber helps to minimize the perturbations connected with the return flow. Also notice, in Figure 1 (a), the immersed filtering panel also used to damp-out flow perturbations within the water tank. On the other hand, the rigid panel which covers almost the complete surface of the water, which can be noticed in Figure 2, is used to avoid wave sloshing in the reservoir.

Figure 2. *Experimental configuration with two articulated pipes*

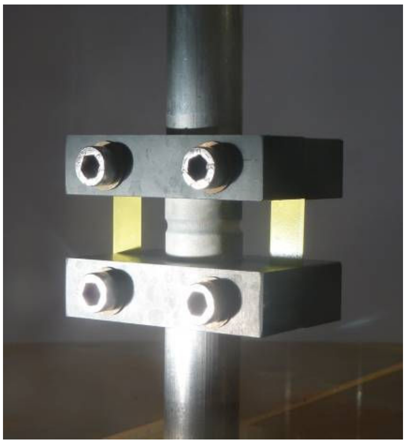

Figure 3. *Detail of a pipe articulation*

Figure 3 shows in detail one of the two identical devices designed for articulating the pipes. These consist in two PVC paired fixtures, which are bolted tightly embracing the aluminum pipes near the pipe extremities. The PVC jaw pairs also assemble, along the axial direction, two symmetrical rectangular stainless steel blades (with a few tenth of millimeter thickness), which enforce the planar motion of the pipes, while introducing a comparatively low angular stiffness to the articulation. Notice, in Figure 3, the thin latex sealing cover, tightened to the pipes through the PVC fixtures.

Figure 4. *Electromagnetic lifting device (left) and eddy-current Kaman displacement transducer (right)*

Figure 5. *Baffled pipe with a smooth rounded water inlet, for a low value of the singular pressure loss*

For each flow velocity, the transient free vibrations of the system released from a small angular displacement were digitized using a Siglab 4 channel acquisition system, and then recorded and analyzed. Figure 4 highlights the upper part of the test section, showing in the left the electromechanical device used for the releasing initial position of the tubes. In the right one can see the Kaman eddy-current displacement transducer used to measure the response. A laser vibrometer was also pointed to the lower part of the mobile ensemble, as shown in Figure 1 (b).

When testing the one-pipe configuration, special attention was paid to evaluate the possible effect of changing the head loss at the inlet. Therefore, two different inlet configurations were tested: (1) the "naked" sharp-edged pipe termination which can be seen in Figure 1 (b); and (2) the baffled pipe termination shown in Figure 5, which presents a well-rounded inlet, with wall radius $r/D_{\text{ext}} \approx 0.25$. The corresponding steady-state loss coefficients, for entering flow, are respectively $K \approx 0.5$ and $K \approx 0.03$ – see Idel'cik (1960).

For most tests, responses were measured at increments $\Delta V_f = 0.1$ m/s of the flow velocity. However, for the experiments using the smooth baffled inlet, a larger velocity increment was adopted. Modal identifications were performed from the post-release free pipe motions using our implementation of the Eigensystem Realization Algorithm (ERA), which is a powerful multi-degree of freedom identification algorithm in the time-domain, see Juang & Pappa (1985) or Juang (1994) for details. In most cases the modal identifications posed no particular problem, except – for tests under normal (expelling) flow – when reaching very high levels of the modal damping and very low values of the modal frequencies, when the time-scales of the oscillatory and damping components of the complex eigenvalues are of the same order of magnitude, and thus difficult to separate.

3 MODELS OF THE TESTED PIPE CONFIGURATIONS

Sketches of the tested one-pipe and two-pipes configurations are shown in Figures 6 and 7, respectively. The dynamics of these flow-structure coupled systems are described by the general formulation:

$$\begin{aligned}&\left[[M_s]+[M_{fe}]+[M_{fi}]\right]\{\ddot{\Theta}\}+\\&+\left[[C_s]+[C_{fe}]+[C_{fi}(V_f)]\right]\{\dot{\Theta}\}+\\&+\left[[K_s]+[K_{fe}]+[K_{fi}(V_f)]\right]\{\Theta\}=\{\mathbf{0}\}\end{aligned} \tag{2}$$

where matrices $[M_s]$, $[C_s]$ and $[K_s]$ stand for the inertia, dissipation and stiffness of the structural components, respectively, $[M_{fe}]$, $[C_{fe}]$ and $[K_{fe}]$ stand for the added mass, dissipation and stiffness effects stemming from the external stagnant fluid, while $[M_{fi}]$, $[C_{fi}(V_f)]$ and $[K_{fi}(V_f)]$ stand for the added mass, the Coriolis and the centrifugal coupling effects stemming from the internal flow. For the single-degree of freedom one-pipe system, the generalized motion is $\{\Theta(t)\} \equiv \theta_1(t)$, while for the system with two articulated pipes $\{\Theta(t)\} \equiv \langle \theta_1(t), \theta_2(t) \rangle^T$. The various terms of equation (1) which are non-dependent on the flow velocity V_f have been detailed in Annex A for the single-pipe system, and in Annex B for the two-pipe system.

Finally, the crucial velocity-dependent flow-coupling terms $[C_i(V_f)]$ and $[K_i(V_f)]$, which depend on the assumed inflow model, are developed in the companion paper, Part 1.

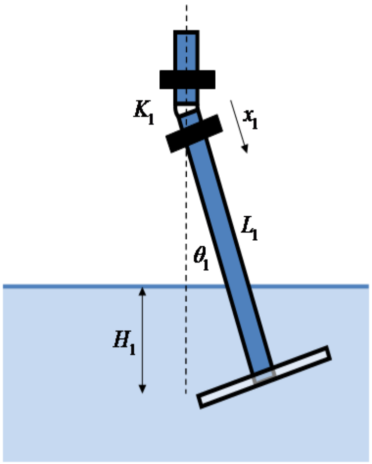

Figure 6. *One-pipe tested configuration*

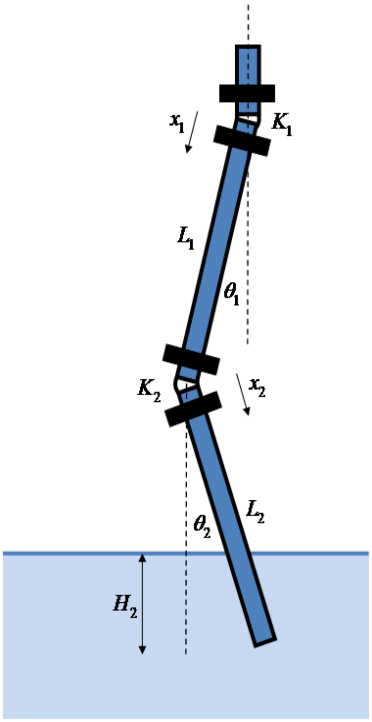

Figure 7. *Two-pipes tested configuration*

A) Normal, expelling flow: For our one-pipe and two-pipes articulated systems, the Coriolis and centrifugal terms stemming from the classic formulation are:

(A-1) One-pipe system, expelling flow:

$$C_i(V_f) = m_f V_f L_1^2 \quad ; \quad K_i(V_f) = 0 \tag{3}$$

(A-2) Two-pipes system, expelling flow:

$$\begin{aligned} \left[C_i(V_f)\right] &= m_f V_f L_1^2 \begin{bmatrix} 1 & 2\Lambda \\ 0 & \Lambda^2 \end{bmatrix} \\ \left[K_i(V_f)\right] &= m_f V_f^2 L_1 \begin{bmatrix} -1 & 1 \\ 0 & 0 \end{bmatrix} \end{aligned} \tag{4}$$

where $m_f = \rho_f S_f$ is the fluid mass per unit length, with ρ_f the fluid density and $S_f = \pi\left(D_{\text{int}}/2\right)^2$ the pipe internal cross-section.

B) Reversed, aspirating flow: As amply discussed in the companion paper, the coupling terms $\left[C_i(V_f)\right]$ and $\left[K_i(V_f)\right]$ for aspirating flows are strongly dependent on the assumed inlet boundary conditions, which were quantified in terms of parameters α, β, γ and π_p. Referring to the theoretical analysis of Part 1, we obtain the following *net* Coriolis and centrifugal matrices (accounting for the boundary conditions), in connection with these modeling parameters:

(B-1) One-pipe system, aspirating flow:

$$C_i(V_f) = -m_f \left|V_f\right| L_1^2 \gamma \quad ; \quad K_i(V_f) = m_f V_f^2 L_1 \left(\beta - 1\right) \tag{5}$$

(B-2) Two-pipes system, aspirating flow:

$$\begin{aligned} \left[C_i(V_f)\right] &= m_f \left|V_f\right| L_1^2 \begin{bmatrix} -\gamma & -\left(1+\gamma\right)\Lambda \\ \left(1-\gamma\right)\Lambda & -\gamma\Lambda^2 \end{bmatrix} \\ \left[K_i(V_f)\right] &= m_f V_f^2 L_1 \left\{ \begin{aligned} &\left(1+\frac{\pi_p}{2}\right)\begin{bmatrix} -1 & 1 \\ 0 & 0 \end{bmatrix} + \\ &+\begin{bmatrix} 1-\alpha & \beta-1 \\ 0 & \Lambda\left(\beta-\alpha\right) \end{bmatrix} \end{aligned} \right\} \end{aligned} \tag{6}$$

where $\Lambda = L_2 / L_1$.

As an illustration, referring to two interesting non-reversible particular scenarios, we obtain (assuming $\pi_p = -2$):

(B1) Inlet flow velocity along the axial direction of the moving pipe:

(B1-1) One-pipe system: $\left(\beta = 1, \gamma = 0\right)$

$$C_i(V_f) = 0 \quad ; \quad K_i(V_f) = 0 \tag{7}$$

(B1-2) Two-pipes system: $\left(\alpha = \beta = 1, \gamma = 0\right)$

$$\begin{aligned} \left[C_i(V_f)\right] &= -m_f \left|V_f\right| L_1^2 \begin{bmatrix} 0 & \Lambda \\ -\Lambda & 0 \end{bmatrix} \\ \left[K_i(V_f)\right] &= \left[\mathbf{0}\right] \end{aligned} \tag{8}$$

(B2) Inlet flow velocity along the vertical direction of the undeflected pipe:

(B2-1) One-pipe system: $\left(\beta = \gamma = 0\right)$

$$C_i(V_f) = 0 \quad ; \quad K_i(V_f) = -m_f V_f^2 L_1 \tag{9}$$

(B2-2) Two-pipes system: $\left(\alpha = 1, \beta = \gamma = 0\right)$

$$\begin{aligned} \left[C_i(V_f)\right] &= -m_f \left|V_f\right| L_1^2 \begin{bmatrix} 0 & \Lambda \\ -\Lambda & 0 \end{bmatrix} \\ \left[K_i(V_f)\right] &= m_f V_f^2 L_1 \begin{bmatrix} 0 & -1 \\ 0 & -\Lambda \end{bmatrix} \end{aligned} \tag{10}$$

As pointed in Part 1, both these scenarios lead to a gyroscopic coupling from the aspiring fluid, the last one also implying a follower force effect. These different flow models are easily implemented in the general formulation (2), together with the relevant terms pertaining to the structure and the external stagnant flow computed in Annexes A and B. Then, as a function of the flow velocity, theoretical predictions of the modal parameters $\omega_n(V_f)$ and $\zeta_n(V_f)$ are computed from the following eigen-formulation, in terms of the global matrices of the system:

$$\left[-\omega^2\left[\,M_T\,\right] + i\omega\left[C_T(V_f)\right] + \left[K_T(V_f)\right]\right]\left\{\bar{\Theta}\right\} = \left\{\mathbf{0}\right\} \tag{11}$$

which is conveniently re-written in the standard, first-order, state-space form.

4 RESULTS FOR THE ONE-PIPE CONFIGURATION

The relevant parameters for this test rig were given in Section 2, and the corresponding dynamical coefficients are detailed in Annex A. The stiffness and dissipation coefficients of the articulation, K_1 and C_1, are inferred from the identified modal frequency and damping in air, $f_s = 2.1\ \text{Hz}$ and $\zeta_s = 4.0\ \%$. Then, dissipation from the external fluid C_{fe} is extracted from the modal parameters in stagnant water, $f_a = 1.1\ \text{Hz}$ and $\zeta_a = 5.0\ \%$. From these results, we may compute the following reduced parameters defined in Part 1, for this test configuration:

$$\Gamma = \frac{\left(M_s + M_a\right) g L_1}{2K_1} \quad ; \quad \mu_a = \frac{M_s}{M_s + M_a} \quad ; \quad V_R = \frac{V\sqrt{\mu_a}}{\omega_a L_1} \tag{12}$$

where subscript s refers to the effects stemming from all moving structural elements and subscript a to those stemming from the interior and external fluid, under no-flow conditions. The values obtained are: $\Gamma = 0.43$, $\mu_a = 0.35$ and $V_R = 0 \sim \pm 0.82$.

$\left(\beta = 1, \gamma = 0\right)$

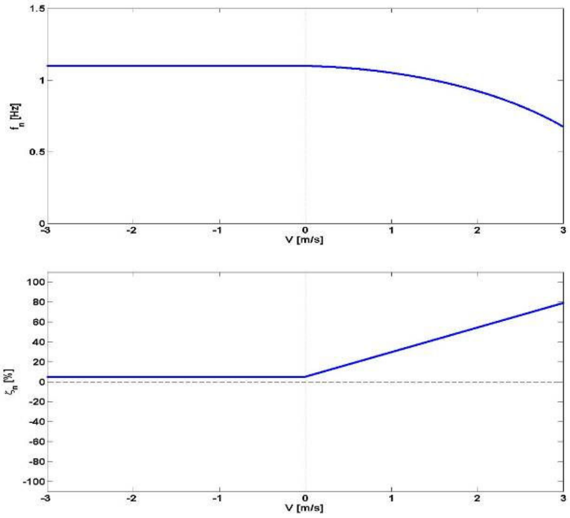

$\left(\beta = \gamma = 0\right)$

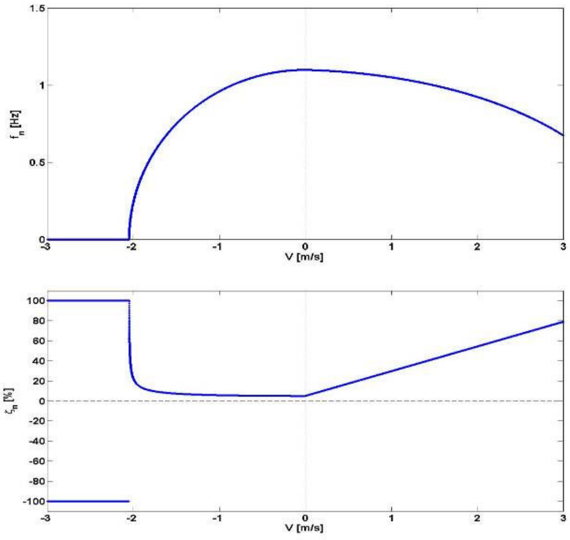

Figure 8. *Predicted dynamics of the one-pipe configuration, for inlet flow scenarios B1 and B2*

The theoretical modal frequencies and damping values for our experimental rig are plotted in Figure 8, as a function of the flow velocity, for the two previously sketched scenarios. For expelling flow $(V_f > 0)$, the dramatic damping effect of the Coriolis coupling force is obvious. For aspirating flow $(V_f < 0)$, as predicted from theory, model B1 is totally insensitive to the reverse flow, while model B2 produces a severe decrease in frequency and ultimately a divergence instability.

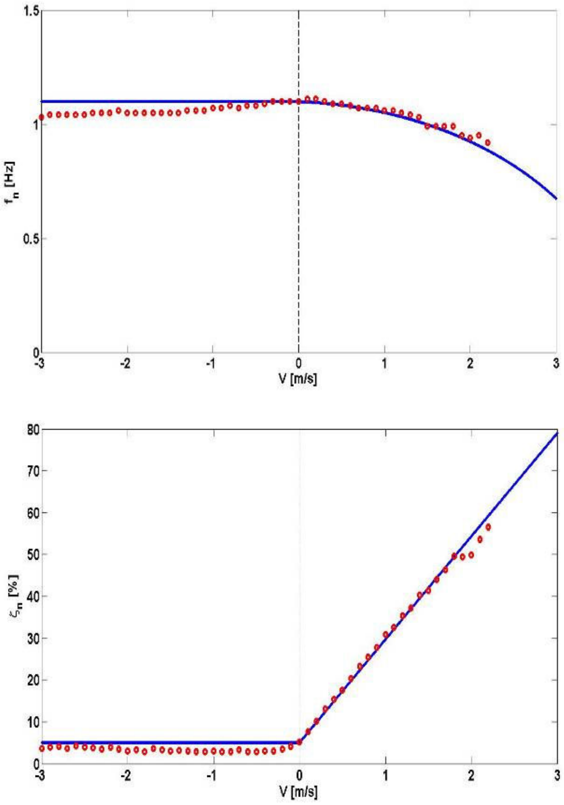

Figure 9. *Experimental results of the one-pipe tested configuration* and theoretical predictions from scenario B1 ($\beta = 1$ and $\gamma = 0$)

The experimental results obtained are shown in Figure 9, and they clearly tend to follow scenario B1, where $\beta = 1$ and $\gamma = 0$, at least to first order. Therefore, such theoretical model was the one chosen to be superimposed to the experimental data, with quite satisfactory results. One may notice, for the normal expelling flow, that the modal damping increases as predicted, up to magnitudes such that the modal identification techniques become unreliable. For aspirating flows, although the "big picture" clearly follows the predictions of the inlet scenario B1, one may notice a slight progressive decrease of the modal frequencies as the suction velocity increases. Also notice that, although essentially flow-independent, the damping values are also slightly lower under suction than at zero flow velocity.

These observations may stem from some sensitivity of the pipe articulation and delicate seal to the flow conditions. However, they may also be due to small departures of the inlet flow field from the modeling scenario B1, which was assumed for the theoretical predictions in Figure 9. Actually, as discussed in Part 1 and further substantiated in the following section, such variations may be accommodated by small adjustments in the inlet flow modeling parameters**.**

We noted earlier that, when testing the one-pipe configuration, special attention was paid to check that the head loss at the aspirating inlet has no effect on the pipe response. Indeed, as expected, a similar insensitivity to the aspirating flow was displayed by the baffled with a rounded inlet shown in Figure 5.

5 RESULTS FOR THE TWO-PIPES CONFIGURATION

We now turn to the two-pipe configuration, for which the dynamical coefficients are detailed in Annex B. Again, the stiffness and dissipation coefficients of the articulations, K_1, K_2, C_1 and C_2, are inferred from the identified modal frequencies and damping in air, $f_{s1} = 0.90\ \text{Hz}$, $f_{s2} = 2.3\ \text{Hz}$, $\zeta_{s1} = 0.7\ \%$ and $\zeta_{s2} = 3.0\ \%$. Then, the dissipation matrix from the external fluid $\left[C_{fe}\right]$ was empirically adjusted in order to reproduce the modal parameters in stagnant water, which were $f_{a1} = 0.67\ \text{Hz}$, $f_{a2} = 1.7\ \text{Hz}$, $\zeta_{a1} = 2.9\ \%$ and $\zeta_{a2} = 2.2\ \%$.

The theoretical modal frequencies and damping values of our experimental rig are plotted in Figure 10, as a function of the flow velocity, for the two previously described inlet flow scenarios, B1 $(\alpha=\beta=1, \gamma=0)$ and B2 $(\alpha=1, \beta=\gamma=0)$. Comparison of these predictions with the experimentally identified modes shows that the modeling hypothesis B1 is overall much better suited. Therefore, Figure 11 displays the experimental results obtained from the two-pipes experiments. These are, again, superimposed with the theoretical predictions using the flow inlet conditions of scenario B1 $(\alpha=\beta=1, \gamma=0)$. Under normal outflow conditions, the theoretical model copes with the experimental results in a satisfactory manner, as expected. Under aspirating flow, the agreement between the experimental and predicted modal frequencies is remarkable, for both modes.

Concerning damping, values for the first mode remain almost insensitive to the reverse flow, and this behavior seems to be well captured by this theoretical model. However, as highlighted in Figure 12, for the higher-frequency mode, experimental results display a slow but clear decrease of damping as the suction velocity increases. This progressive lowering of the second mode damping is not displayed by the inlet parameters of the basic scenario B1, which also predicts little sensitivity of damping to the inflow velocity.

At this level of subtlety in the behavior of the system damping, the freedom allowed by the general formulation (6) becomes quite valuable. Indeed, taking scenario B1 as the basic framework, small changes in the model parameters α, β and γ barely affect the analytically predicted modal frequencies, however they have a definite influence on the system modal damping.

This is clearly attested by comparing the modal damping predictions from parameters $\alpha = \beta = 1$ and $\gamma = 0$ (the basic scenario B1), shown in Figure 12, with those stemming from the slightly modified scenario provided by parameters $\alpha = 1$, $\beta = 0.95$ and $\gamma = 0.02$, which are presented in Figure 13. As stated before, the modal frequencies of this modified scenario are virtually those pictured in Figure 11. Concerning damping, notice that, although still not fitting perfectly the experimental data, the theoretical values from the modified scenario are nevertheless plausible for the first mode data, while clearly defining the decreasing trend of the second mode data.

$(\alpha=\beta=1, \gamma=0)$

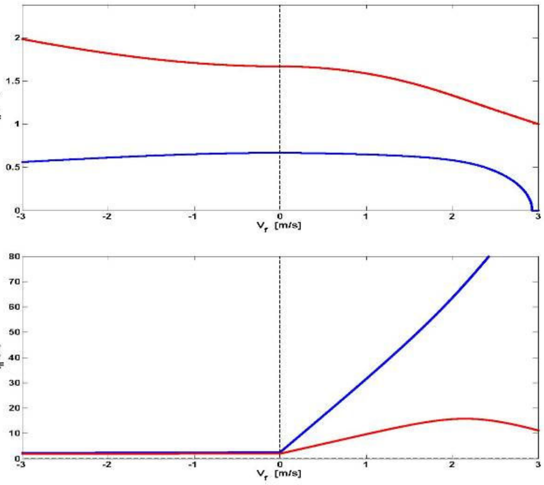

$(\alpha=1, \beta=\gamma=0)$

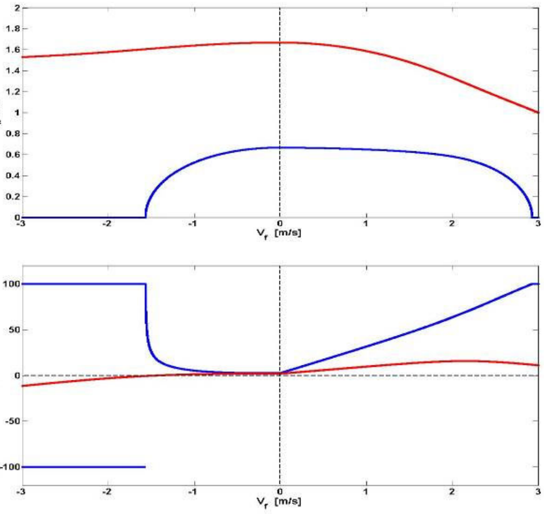

Figure 10. *Predicted dynamics of the one-pipe configuration, for inlet flow scenarios B1 and B2*

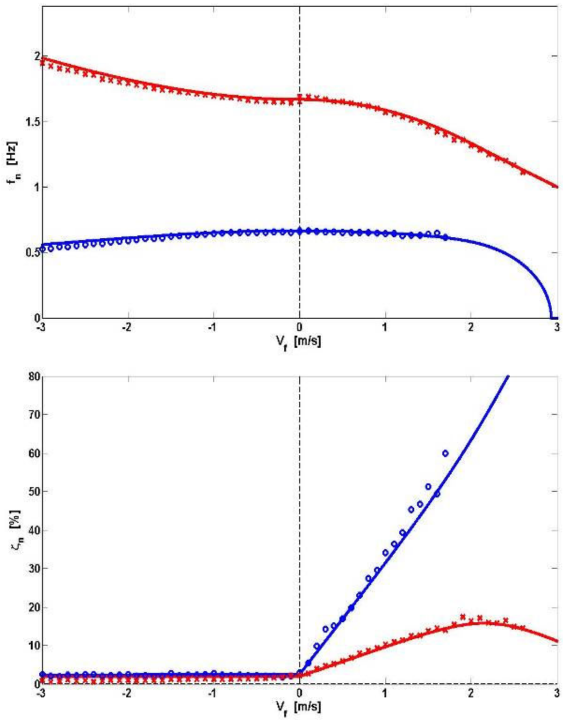

Figure 11. *Experimental results of the two-pipes tested configuration and theoretical predictions from scenario B1 (* $\alpha = \beta = 1$ *and* $\gamma = 0$ *)*

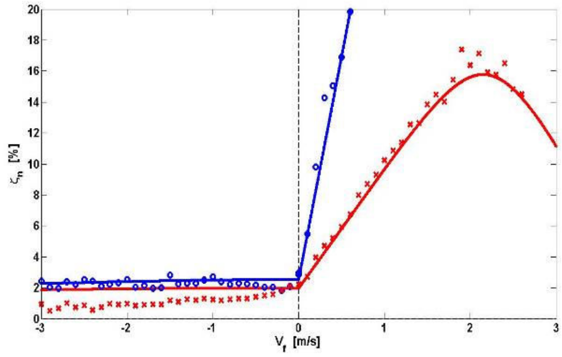

Figure 12. *Detail of the measured and computed damping for the two-pipes tested configuration using scenario B1 (* $\alpha = \beta = 1$ *and* $\gamma = 0$ *)*

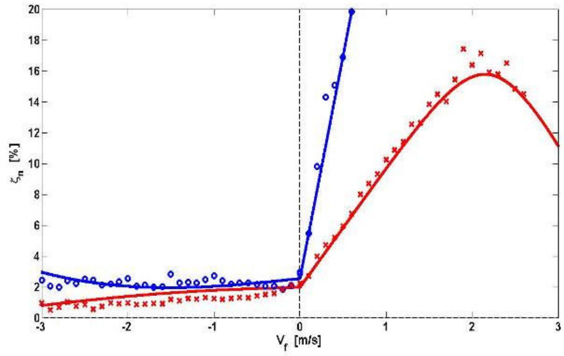

Figure 13. *Detail of the measured and computed damping for the two-pipes tested configuration using a slightly modified scenario from B1 (* $\alpha = 1$, $\beta = 0.95$ and $\gamma = 0.02$)

6 CONCLUSION

In the companion paper, Axisa (2010) devised a logical experimental set-up and testing strategy in order to highlight the dynamical effects of the aspirating fluid boundary conditions. An experimental rig was designed and built in order to validate the analysis of Part 1. Two configurations of partly immersed articulated pipes were tested, both for normal (expelling) and for reversed (aspirating) flows. The experimental results presented pertain to the following pipe configurations: (a) One articulated pipe, with either a common protruding or a rounded baffled free end; and (b) Two articulated pipes with equal lengths. For all flow velocities modal identifications were performed from the measured system responses.

The results obtained under normal flow are in good agreement with the theoretical model originally developed by Benjamin (1961), which is also reviewed in Part 1. For the single articulated pipe, the Coriolis force term leads to a steady increase of damping with the flow velocity, modal frequency being significantly affected only near critical damping. For the two articulated pipes configuration, both the Coriolis and centrifugal flow terms are significant, leading to large changes in both modal frequencies and damping. Although the available flow velocity was insufficient to reach instability boundaries, the results obtained closely follow the classic theoretical model in the velocity range explored.

The most interesting results from our experiments obviously concern aspirating flows. In agreement with previous investigations, the dynamical behavior observed clearly demonstrates that, for aspirating flows, the relevant flow/structure theoretical model must be radically different from the classic formulation which applies to normal flows. Following the discussion of the companion paper, it was found that one-pipe configurations are insensitive to aspirating flows, irrespectively of the pipe termination geometry, showing that the Coriolis force term is canceled exactly by the term arising from the change in momentum of the flow entering the pipe at the free end. Among the three hypothetical inflow scenarios suggested by Païdoussis et al (2005), the one labeled here as (B1), such that the inlet flow velocity lays along the axial direction of the moving pipe with no tangential component, supports most of the findings from the present experiments. Such modeling assumption leads to near-perfect predictions of the one-pipe system dynamics, which remains almost insensitive to the aspirating flow. Furthermore, when drastically changing the flow entrance head loss – by testing a pipe with a baffled rounded inlet – the qualitative dynamics of the systems were not affected whatsoever, as theoretically expected.

The experimental results from the two-pipe configuration, are somewhat sensitive to the aspirating flow velocity. Again, results show that the system dynamics are mostly controlled by the inflow momentum change, as already highlighted by the one-pipe tests. Both identified modal frequencies of the two-pipes system and the first mode damping, as a function of the flow velocity, closely follow the theoretical predictions using this inlet scenario. However, a discrepancy was observed concerning the trend of the second mode damping, which decreases somewhat as the aspirating velocity increases, a result which is not explained from the basic flow assumption B1. Nevertheless, we show that *small* adjustments in the parameters of the inlet flow model produce significant changes in the computed modal damping of the system, while barely changing the modal frequencies. These parameters appear, therefore, as instrumental for understanding the subtle damping behavior and stability of aspirating pipe systems.

NOMENCLATURE

C_1 , C_2	Dissipation of the articulations [Nm s/rad]
$\left[C_{fe}\right]$	Damping matrix from the external fluid
$\left[C_{fi}(V_f)\right]$	Damping matrix from the internal flow
$\left[C_s\right]$	Damping matrix of the structure
$\left[C_T(V_f)\right] = \left[C_s\right] + \left[C_e\right] + \left[C_i(V_f)\right]$	
D_{int} , D_{ext}	Internal and external pipe diameters [m]
g	Gravity acceleration [m/s^2]
H_1 , H_2	Immersed height of the pipes [m]
K	Head loss coefficient at pipe inlet
K_1 , K_2	Stiffness of the articulations [Nm/rad]
$\left[K_{fe}\right]$	Stiffness matrix from the external fluid
$\left[K_{fi}(V_f)\right]$	Stiffness matrix from the internal flow
$\left[K_s\right]$	Stiffness matrix of the structure
$\left[K_T(V_f)\right] = \left[K_s\right] + \left[K_e\right] + \left[K_i(V_f)\right]$	
L_1 , L_2	Pipe lengths [m]
m_f	Internal fluid mass per unit length [kg/m]
M_1 , M_2	Pipe masses [kg]
$\left[M_{fe}\right]$	Inertia matrix from the external fluid
$\left[M_{fi}\right]$	Inertia matrix from the internal fluid
$\left[M_s\right]$	Inertia matrix of the structure
$\left[M_T\right] = \left[M_s\right] + \left[M_e\right] + \left[M_i\right]$	
r	Wall radius for the baffled pipe inlet [m]
S_f	Pipe internal cross-section [m^2]
T	Kinetic energy [J]
V	Potential energy [J]
$V_f > 0$	Expelling axial pipe velocity [m/s]
$V_f < 0$	Aspirating axial pipe velocity [m/s]
ρ_f	Fluid density [kg/m^3]
ρ_s	Structure density [kg/m^3]
α , β , γ	Parameters connected with the inlet velocity
π_p	Inlet pressurization coefficient
$\theta_1(t), \theta_2(t)$	Angular pipe motions [rad]

REFERENCES

Axisa, F. (2010), "Flow conditions at the inlet of aspirating pipes: Part 1 – Theoretical Analysis", submitted for presentation at the *7th International Symposium on Fluid-Structure Interaction, Flow-Sound Interaction, Flow-Induced Vibration and Noise*, August 1-4th, 2010, Montreal, Canada.

Benjamin, T.B. (1961a), "Dynamics of a system of articulated pipes conveying fluid : 1 – Theory", *Proceedings of the Royal Society A*, Vol. 261, pp. 457-486.

Benjamin T.B. (1961b), "Dynamics of a system of articulated pipes conveying fluid : 2 - Experiments", *Proceedings of the Royal Society A*, Vol. 261, pp. 487-499.

Berg, R.E., Collier, M.R. (1989), "The Feynman inverse sprinkler problem: A demonstration and quantitative analysis", *American Journal of Physics*, Vol. 57, pp. 654-657.

Collier, M.R., Berg, R.E., Ferrel, R.A. (1991), "The Feynman inverse sprinkler problem: A detailed kinematic study", *American Journal of Physics*, Vol. 59, pp. 349-355.

Feynman, R. (1985), "Surely you're joking Mr. Feynman", Norton, New York, USA.

Giacobbi, D.B. (2007), "A numerical and experimental study of the dynamics of aspirating cantilever pipes", *Undergraduate honours thesis*, Department of Mechanical Engineering, McGill University, Montreal, Canada.

Hongwu, C., Junji, T. (1996), "Effect of boundary conditions on the stability of a cantilever pipe discharging and aspirating fluid", *JSME International Journal (Series C)*, Vol. 39, pp. 20-24.

Hsu, L. (1988), "Inverse sprinklers: Two simple experiments and the resolution of the Feynman-Forrester conflict", *American Journal of Physics*, Vol. 56, pp. 307-308.

Idel'cik, I.E. (1960), "Memento des pertes de charge" (French translation from the Russian, 1969), *Eyrolles*, Paris, France.

Juang, J.N., Pappa, R.S. (1985), "An eigensystem realization algorithm for modal parameter identification and model reduction", *Journal of Guidance, Control and Dynamics*, Vol. 8, pp. 620–627.

Juang, J.N. (1994), "Applied System Identification", Prentice-Hall, Englewood Cliffs, USA.

Kuiper, G.L., Metrikine, A.V., Battjes, J.A. (2007), "A new time-domain drag description and its influence on the dynamic behavior of a cantilever pipe conveying fluid", *Journal of Fluids and Structures*, Vol. 23, pp. 429-445.

Kuiper, G.L., Metrikine, A.V. (2008), "Experimental investigation of dynamic stability of a cantilever pipe aspirating fluid", *Journal of Fluids and Structures*, Vol. 24, pp. 541-558.

Lindgren, E.R. (1990), "The transport momentum theorem", *American Journal of Physics*, Vol. 58, pp. 352-357.

Païdoussis, M.P. (1998), "Fluid-structure interactions: Slender structures and axial flow", Academic Press, London, UK.

Païdoussis, M.P., Semler, C., Wadham-Gagnon, M. (2005), "A reappraisal of why aspirating pipes do not flutter at infinitesimal flow", *Journal of Fluids and Structures*, Vol. 20, pp. 147-156.

Païdoussis, M.P., Tétreault-Friend, M. (2009), "Aspirating cantilevers and reverse sprinklers", *American Journal of Physics*, Vol. 77, pp. 349-353.

Rinaldi, S. (2009), "Experiments on the dynamics of cantilevered pipes subjected to internal and/or external axial flow", *M.Eng. thesis*, Department of Mechanical Engineering, McGill University, Montreal, Canada.

ANNEX A: FORMULATION FOR THE TESTED ONE-PIPE ARTICULATED CONFIGURATION

The conservative dynamical equations for the experimental configurations, under no flow conditions, may be conveniently obtained using Lagrange formulation:

$$\frac{\partial}{\partial t}\left(\frac{\partial T}{\partial \dot{\theta}_n}\right)-\frac{\partial T}{\partial \theta_n}+\frac{\partial V}{\partial \theta_n}=0 \quad ; \quad n=1,2,... \qquad (13)$$

where T and V are the kinetic and potential energies of the system, respectively. The kinetic energy is given as a sum of the following terms:

$$T=T_1+T_a+T_{fi}+T_{fe} \qquad (14)$$

where T_1 pertains to the pipe T_a to the articulation fixture, T_{fi} to the internal fluid and T_{fe} to the external fluid. With respect to the system shown in Figure 6, we have:

$$T_1=\frac{1}{2}\int_0^{L_1}\rho_s\left(S_{\text{ext}}-S_{\text{int}}\right)\left(\dot{\theta}_1 x_1\right)^2 dx_1=\frac{1}{6}M_1 L_1^2\dot{\theta}_1^2 \qquad (15)$$

where the structural mass is:

$$M_1=\rho_s\left(S_{\text{ext}}-S_{\text{int}}\right)L_1 \qquad (16)$$

with:

$$S_{\text{ext}}=\pi\left(D_{\text{ext}}/2\right)^2 \quad ; \quad S_{\text{int}}=\pi\left(D_{\text{int}}/2\right)^2 \qquad (17)$$

On the other hand, $m_a = 70\text{ g}$ is half the mass of the mobile articulation fixture tightened to the pipe, which is modeled as a point mass at location $x_1=\ell_a=15\text{ mm}$, hence:

$$T_a=\frac{1}{2}m_a\ell_a^2\dot{\theta}_1^2 \qquad (18)$$

For the internal fluid, under no flow, we have:

$$T_{fi}=\frac{1}{2}\int_0^{L_1}\rho_f S_{\text{int}}\left(\dot{\theta}_1 x_1\right)^2 dx_1=\frac{1}{6}M_i L_1^2\dot{\theta}_1^2 \qquad (19)$$

where:

$$M_i=\rho_f S_{\text{int}}L_1 \qquad (20)$$

while for the external fluid:

$$T_{fe}=\frac{1}{2}\int_{L_1-H_1}^{L_1}\rho_f S_{\text{ext}}\left(\dot{\theta}_1 x_1\right)^2 dx_1=\frac{1}{2}M_e\left(L_1^2-L_1H_1+\frac{1}{3}H_1^2\right)\dot{\theta}_1^2 \qquad (21)$$

where:

$$M_e=\rho_f S_{\text{ext}}H_1 \qquad (22)$$

Turning to the potential energy, we have:

$$V=V_1^k+V_1^g+V_a^g+V_{fi}^g+V_{fe}^b \qquad (23)$$

were V_1^k stems from the articulation stiffness, V_1^g the tube weight, V_a^g the articulation weight, V_{fi}^g the internal fluid weight and V_{fe}^b from the external fluid buoyancy effect. Hence:

$$V_1^k=\frac{1}{2}K_1\theta_1^2 \qquad (24)$$

$$V_1^g=gM_1\frac{L_1}{2}\frac{\theta_1^2}{2}=\frac{1}{4}gM_1L_1\theta_1^2 \qquad (25)$$

$$V_a^g=\frac{1}{2}gm_a\ell_a\theta_1^2 \qquad (26)$$

$$V_{fi}^g=\frac{1}{4}gM_iL_1\theta_1^2 \qquad (27)$$

$$V_{fe}^b=-g\rho_f S_{\text{ext}}H_1\left(L_1-\frac{H_1}{2}\right)\frac{\theta_1^2}{2}=-\frac{1}{2}gM_e\left(L_1-\frac{H_1}{2}\right)\theta_1^2 \qquad (28)$$

From (13)-(28) we obtain, for the general equation (2), the following coefficients not related to the internal flow:

$$M_s=\frac{1}{3}M_1L_1^2+m_a\ell_a^2$$

$$M_{fe}=M_e\left(L_1^2-L_1H_1+\frac{1}{3}H_1^2\right) \qquad (29)$$

$$M_{fi}=\frac{1}{3}M_iL_1^2$$

and:

$$K_s=K_1+\frac{1}{2}gM_1L_1+gm_a\ell_a$$

$$K_{fe}=-gM_e\left(L_1-\frac{H_1}{2}\right) \qquad (30)$$

$$K_{fi}(0)=\frac{1}{2}gM_iL_1$$

Furthermore, we must add the empirical dissipation terms:

$$C_s = C_1 \quad ; \quad C_{fe} = C \quad ; \quad C_{fi}(0) = 0 \tag{31}$$

were the structural coefficient C_1 and the external fluid dissipation coefficient C_{fe} are identified from the tests in air and in water, with no flow, respectively.

ANNEX B: FORMULATION FOR THE TESTED TWO-PIPE ARTICULATED CONFIGURATION

Proceeding as before, with respect to the configuration shown in Figure 7, we now have:

$$T = T_1 + T_2 + T_a + T_b + T_c + T_{fi} + T_{fe} \tag{32}$$

were T_a to T_c relate to the identical elements of the articulation fixtures $m_a = m_b = m_c$, which are attached to the tubes, respectively at $x_1 = \ell_a$, $x_1 = L_1 - \ell_a$ and $x_2 = \ell_a$. The various kinetic energy terms read:

$$T_1 + T_2 = \frac{1}{2} M_1 L_1^2 \left[\left(\frac{1}{3} + \Lambda \right) \dot{\theta}_1^2 + \Lambda^2 \dot{\theta}_1 \dot{\theta}_2 + \frac{\Lambda^3}{3} \dot{\theta}_2^2 \right] \tag{33}$$

were we define $\Lambda = L_2 / L_1$, as in Part 1.

$$T_a + T_b + T_c = \frac{1}{2}\left(m_a \ell_a^2 + m_b \ell_b^2 + m_c L_1^2 \right) \dot{\theta}_1^2 + m_c L_1 \ell_c \dot{\theta}_1 \dot{\theta}_2 + \frac{1}{2} m_c \ell_c^2 \dot{\theta}_2^2 \tag{34}$$

$$T_{fi} = \frac{1}{2} M_i L_1^2 \left[\left(\frac{1}{3} + \Lambda \right) \dot{\theta}_1^2 + \Lambda^2 \dot{\theta}_1 \dot{\theta}_2 + \frac{\Lambda^3}{3} \dot{\theta}_2^2 \right] \tag{35}$$

$$\begin{aligned} T_{fe} &= \frac{1}{2} \rho_f S_e \int_{L_2 - H_2}^{L_2} \left(L_1 \dot{\theta}_1 + x_2 \dot{\theta}_2 \right)^2 dx_2 \\ &= \frac{1}{2} M_e \begin{bmatrix} L_1^2 \dot{\theta}_1^2 + L_1 \left(2\Lambda L_1 - H_2 \right) \theta_1 \theta_2 + \\ + \left(\Lambda^2 L_1^2 - \Lambda L_1 H_2 + \frac{1}{3} H_2^2 \right) \dot{\theta}_2^2 \end{bmatrix} \end{aligned} \tag{36}$$

where:

$$M_e = \rho_f S_{\text{ext}} H_2 \tag{37}$$

For the potential energy, we have:

$$V = V_1^k + V_2^k + V_1^g + V_2^g + V_a^g + V_b^g + V_c^g + V_{fi}^g + V_{fe}^b \tag{38}$$

with:

$$V_1^k + V_2^k = \frac{1}{2}\left(K_1 + K_2 \right) \theta_1^2 - K_2 \theta_1 \theta_2 + \frac{1}{2} K_2 \theta_2^2 \tag{39}$$

$$V_1^g + V_2^g = \frac{1}{4} g M_1 L_1 \left[\left(1 + 2\Lambda \right) \theta_1^2 + \Lambda^2 \theta_2^2 \right] \tag{40}$$

$$V_a^g + V_b^g + V_c^g = \frac{1}{2} g \left(m_a \ell_a + m_b \ell_b + m_c L_1 \right) \theta_1^2 + \frac{1}{2} g m_c \ell_c \theta_2^2 \tag{41}$$

$$V_{fi}^g = \frac{1}{4} g M_i L_1 \left[\left(1 + 2\Lambda \right) \theta_1^2 + \Lambda^2 \theta_2^2 \right] \tag{42}$$

$$V_{fe}^b = -\frac{1}{2} g M_e \left[L_1 \theta_1^2 + \left(\Lambda L_1 - \frac{H_2}{2} \right) \theta_2^2 \right] \tag{43}$$

Then, from (13) and (32)-(43) we obtain the following coefficient matrices:

$$\begin{gathered} \left[M_s \right] = \frac{1}{3} M_1 L_1^2 \begin{bmatrix} 1 + 3\Lambda & \dfrac{3\Lambda^2}{2} \\ \dfrac{3\Lambda^2}{2} & \Lambda^3 \end{bmatrix} + \begin{bmatrix} m_a \ell_a^2 + m_b \ell_b^2 + m_c L_1^2 & m_c L_1 \ell_c \\ m_c L_1 \ell_c & m_c \ell_c^2 \end{bmatrix} \\ \left[M_{fe} \right] = M_e \begin{bmatrix} L_1^2 & L_1 \left(\Lambda L_1 - \frac{1}{2} H_2 \right) \\ L_1 \left(\Lambda L_1 - \frac{1}{2} H_2 \right) & \Lambda^2 L_1^2 - \Lambda L_1 H_2 + \frac{1}{3} H_2^2 \end{bmatrix} \\ \left[M_{fi} \right] = \frac{1}{3} M_i L_1^2 \begin{bmatrix} 1 + 3\Lambda & \dfrac{3\Lambda^2}{2} \\ \dfrac{3\Lambda^2}{2} & \Lambda^3 \end{bmatrix} \end{gathered} \tag{44}$$

and:

$$\begin{gathered} \left[K_s \right] = \begin{bmatrix} K_1 + K_2 & -K_2 \\ -K_2 & K_2 \end{bmatrix} + \frac{1}{2} g M_1 L_1 \begin{bmatrix} 1 + 2\Lambda & 0 \\ 0 & \Lambda^2 \end{bmatrix} + \\ + g \begin{bmatrix} m_a \ell_a + m_b \ell_b + m_c L_1 & 0 \\ 0 & m_c \ell_c \end{bmatrix} \\ \left[K_{fe} \right] = -g M_e \begin{bmatrix} L_1 & 0 \\ 0 & \Lambda L_1 - \dfrac{H_2}{2} \end{bmatrix} \\ \left[K_{fi}(0) \right] = \frac{1}{2} g M_i L_1 \begin{bmatrix} 1 + 2\Lambda & 0 \\ 0 & \Lambda^2 \end{bmatrix} \end{gathered} \tag{45}$$

and again, we must add the dissipation matrices:

$$\begin{gathered} \left[C_s \right] = \begin{bmatrix} C_1 + C_2 & -C_2 \\ -C_2 & C_2 \end{bmatrix} \quad ; \quad \left[C_{fe} \right] = \begin{bmatrix} C_{11} & C_{12} \\ C_{12} & C_{22} \end{bmatrix} \\ \left[C_{fi}(0) \right] = \left[\mathbf{0} \right] \end{gathered} \tag{46}$$

were the structural coefficients C_1 and C_2 are identified from the tests in air, while the external fluid dissipation $\left[C_{fe} \right]$ is adjusted from the modal parameters identified in stagnant water.